6(2009) 187 – 212

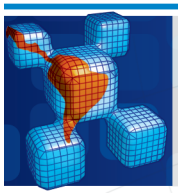

Latin American Journal of Solids and Structures
www.lajss.org

# Two dimensional analysis of inflatable structures by the positional FEM

**Abstract**

This paper presents a simple two dimensional frame formulation to deal with structures undergoing large motions due to dynamic actions including very thin inflatable structures, balloons. The proposed methodology is based on the minimum potential energy theorem written regarding nodal positions. Velocity, acceleration and strain are achieved directly from positions, not displacements, characterizing the novelty of the proposed technique. A non-dimensional space is created and the deformation function (change of configuration) is written following two independent mappings from which the strain energy function is written. The classical Newmark equations are used to integrate time. Dumping and non-conservative forces are introduced into the mechanical system by a rheonomic energy function. The final formulation has the advantage of being simple and easy to teach, when compared to classical counterparts. The behavior of a bench-mark problem (spin-up maneuver) is solved to prove the formulation regarding high circumferential speed applications. Other examples are dedicated to inflatable and very thin structures, in order to test the formulation for further analysis of three dimensional balloons.

**Keywords**

Geometrical non-linear analysis, FEM, Dynamics, Ballons

**Humberto Breves Coda***

Universidade de São Paulo, Departamento de Engenharia de Estruturas, Av. Trabalhador São-Carlense 400, 13570960, São Carlos, São Paulo – Brazil

Received 17 Apr 2009;
In revised form 20 Aug 2009

* Author email: hbcoda@sc.usp.br

## 1 INTRODUCTION

Interesting researches had been developed regarding transient dynamic analysis of flexible structures (frames for instance) undergoing large motions. Simo and Vu Quocs paper [21] describes various different formulations for this purpose. The authors were interested mainly in the rotating beam stiffens due to inertial forces, proving that some previous formulations were unable to reproduce this important property. In that study three valid formulations were cited. The first is the so-called co-rotational formulation, which uses a consistent linearization of the fully non-linear beam theory. It makes use of a "floating frame" that accompanies the overall movement of the rotating bar. The strain measure is of the second-order expansion, using the auxiliary floating frame as a reference, see references [19, 20].

The second one is called exact [21] and uses the fully non-linear strain measurement and a floating frame as an intermediate reference to calculate strains. After that, the achieved strain is rotated to the inertial reference. For both formulations the associated differential equation is achieved and afterwards the standard Galerkin approximation is employed to solve the problem.

The third formulation [15] employs a finite element procedure based on the theorem of minimum potential energy assuming a centerline elongation based on curvilinear co-ordinates and a first order distortion. It is interesting to mention that the majority of dynamic non-linear analyses is made following a co-rotational linearized procedure, where a floating frame reference is present [10–12, 26]. The common point of all cited formulations is the intrinsic relation between strain and displacements, linearized or not, using a floating frame or curvilinear co-ordinates as a reference.

The present study proposes a simple and robust formulation to deal with flexible dynamic structures based on the principle of minimum potential energy and focus its application to very thin structures, namely balloons. It is different from all other approaches as it is based on position description, not displacement, and does not use a floating frame to define strain [8, 9, 13, 14].

The adopted strain measure is commonly known as Green strain [17]. Its natural energetic conjugate is the Second Piola Kirchhoff stress. Quadratic strain energy potential is adopted, resulting a linear relation between stress and strain called Saint-Venant-Kirchhoff constitutive relation. The simplicity of the proposed formulation makes possible to develop curved element of any order of approximation.

This work is devoted to test the proposed formulation in applications regarding very thin inflatable structures (balloons) before starting a dynamic three dimensional generalization. This application is very important, as balloons are the vehicles most used to do researches regarding our environment (earth) and are the ones chosen by spatial agencies as the future vehicles to explore other planets [3]. As far as the authors' knowledge goes, the simulation of this kind of structures adopts membrane approach, as can be seen in several important works, e.g. [2–4] among others. The membrane approach solves wrinkling replacing the wrinkled region by a smooth pseudo-surface, as proposed in [18, 22, 23]. However, the consideration of folds is avoided when adopting the membrane approach.

In this study, considering flexural stiffness, general post-buckling (geometrical non-linear position paths) of very thin 2D structures (balloons) are analyzed. These analyzes open the possibility for further 3D applications, including partially inflatabled balloons and folding. To solve transient problems the Newmark time integrator [1, 9] is employed. The behavior of a bench-mark problem (spin-up maneuver) is presented to prove the accuracy of the formulation. Other examples: The load rate influence in the de-inflation of a free cylindrical balloon (post buckling and folding), the slow de-inflation of a cylindrical balloon over a half-space, the fast inflation and taking off of the same balloon with the presence of the half-space surface and the analysis of balloons shapes depending on the internal pressure pattern.

## 2 STRAIN MEASURE AND SPECIFIC STRAIN ENERGY POTENTIAL

This section summarizes simple concepts used to derive the proposed formulation. The Green strain tensor is derived directly from the gradient of the deformation gradient, represented by letter **A,** given as follows:

$$A_{ij} = \frac{\partial f_i}{\partial x_j} \tag{1}$$

where $f_i$ is deformation function, as depicted in figure 1, and $x_j$ is a coordinate representing variation initial position and $y_i = f_i(x_{(i)})$ represents current position.

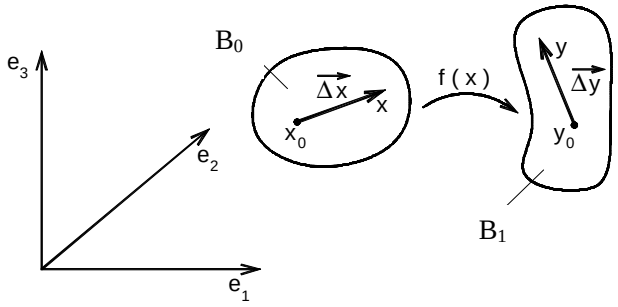


Figure 1 Change of configuration (deformation).

In figure 1 $dx_i$ and $dy_i$ represent an infinitesimal fiber in the initial and current continuum configurations, respectively. Following detailed steps given by [17] including geometrical meanings, the Green strain can be written as:

$$E_{ij} = \frac{1}{2}\left[A_{ki}A_{kj} - \delta_{ij}\right] = \frac{1}{2}\left[C_{ij} - \delta_{ij}\right] \tag{2}$$

In which index notation is adopted. The variables $C_{ij}$ and $\delta_{ij}$ are the right Cauchy stretch tensor and the Kroenecker delta, respectively. The following quadratic strain energy per unit of initial volume is adopted,

$$u_e = \frac{1}{2}E_{ij}C_{ijkl}E_{kl} \tag{3}$$

where $C_{ijk\ell}$ is the forth order elastic tensor. Equation (3) results in he so called Saint-Venant – Kirchhoff constitutive law, relating the second Piola Kirchhoff stress and the Green strain tensor, i.e.:

$$S_{ij} = \frac{\partial u_e}{\partial E_{ij}} = C_{ijkl}E_{kl} \tag{4}$$

where

$$C_{ijkl} = \frac{2G\upsilon}{1-2\upsilon}\delta_{ij}\delta_{kl} + G\left(\delta_{ik}\delta_{jl} + \delta_{il}\delta_{jk}\right) \tag{5}$$

In which $\nu$ is the Poisson ratio. The shear modulus is given by,

$$G = \frac{E}{2(1+\nu)} \tag{6}$$

with $E$ being the well known Young modulus.

The relation among Second Piola Kirchhof stress and the True Stress (Cauchy Stress) is straightforward [6, 17]. For the sake of completeness one recalls that the right Cauchy-Green stretch tensor is positive definite, symmetric and has six independent values [17].

## 3 KINEMATICAL APPROXIMATION AND POSITIONAL MAPPING

This section describes the proposed kinematics for frames. A complete description of the positional technique for solids can be seen in [7]. It is important to note that expressions, simple as presented, are general and comprise curved elements with all approximation orders.

One can approximate positions of the mid-line points of a frame element, see figure 2, by the following mapping.

$$f_i^{m0} = x_i^m(\xi_1, X_{\ell i}) = \phi_\ell(\xi_1) X_{\ell i} \tag{7}$$

$$f_i^{m1} = y_i^m(\xi_1, Y_{\ell i}) = \phi_\ell(\xi_1) Y_{\ell i} \tag{8}$$

where $x_i^m$ is the ith coordinate of a generic point in the mid-line of the frame at initial configuration, $X_{\ell i}$ is the ith coordinate of node $\ell$, $y_i^m$ is the ith coordinate of a generic point in the mid-line of the frame at current configuration, $Y_{\ell i}$ is the ith coordinate of node $\ell$ at current configuration. One can see in figure 2 that $f^{m0}$ is the positional mapping from the auxiliary space to the initial configuration, $f^{m1}$ is the positional mapping from the auxiliary space to the current configuration, $f^m$ is the positional mapping from the initial configuration to the current one (not to be written) and the values $A^{m0}$, $A^{m1}$, $A^m$ are their respective gradients.

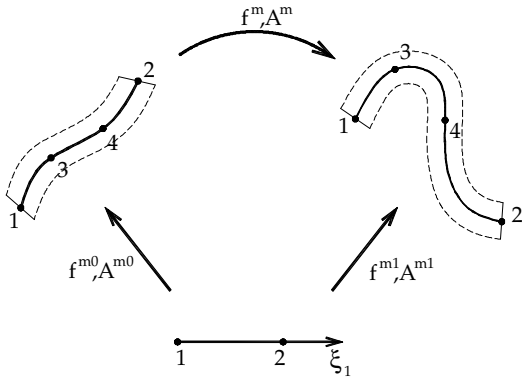


Figure 2 Mid-lines mappings.

To complete the frame kinematics description, for both initial and current configurations, one realizes that the difference between a point out of the mid-line and its correspondent belonging to the mid-line generates position vectors $\vec{g}^o$ or $\vec{g}^1$, see figure 3.

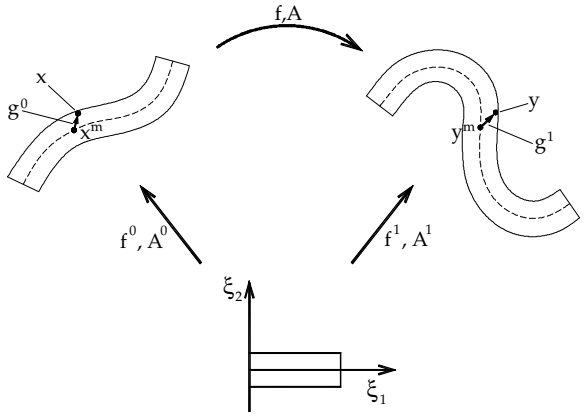


Figure 3 Position vectors.

By the other hand, a general point of the frame can be defined by adding the position vectors to the corresponding mid-line point, i.e.,

$$x_i = x_i^m + g_i^0 \tag{9}$$

$$y_i = y_i^m + g_i^1 \tag{10}$$

Following [5, 7], for constant thickness variation regarding $\xi_2$, as $x_i^m$ and $y_i^m$ has already been parameterized, one writes $g_i^0$ and $g_i^1$ as functions of non-dimensional variables and positional rotation $\theta$, as

$$g_1^0 = \frac{h_0(\xi_1)}{2}\cos(\theta^0(\xi_1))\,\xi_2 \tag{11}$$

$$g_2^0 = \frac{h_0(\xi_1)}{2}\sin(\theta^0(\xi_1))\,\xi_2 \tag{12}$$

$$g_1^1 = \frac{h_0(\xi_1)}{2}\cos(\theta^1(\xi_1))\,\xi_2 \tag{13}$$

$$g_2^1 = \frac{h_0(\xi_1)}{2}\sin(\theta^1(\xi_1))\,\xi_2 \tag{14}$$

where $h_0$, $\theta^0$ and $\theta^1$ are, respectively, the height, initial rotation and final rotation of any cross section along the mid-line of the element.

We will assume that the height of the element is constant and that the cross section rotation is approximated similarly to the mid line positions, as

$$\theta^0(\xi_1) = \phi_\ell(\xi_1)\theta^0_\ell \tag{15}$$

$$\theta^1(\xi_1) = \phi_\ell(\xi_1)\theta^1_\ell \tag{16}$$

where $\theta^j_\ell$ are the cross section rotations for nodal points $\ell$ for initial and current configurations represented by letter $j$.

Introducing equations (15) and (16) into equations (11) trough (14) and then into equations (9) and (10) one achieves the parametric positional mapping from the auxiliary space to the initial configuration ($f^0_i$) and the parametric positional mapping from the auxiliary space to the current configuration ($f^1_i$) as follows:

$$f^0_1 = x_1 = \phi_\ell(\xi_1)X_{\ell 1} + \frac{h_0}{2}\xi_2\cos(\phi_\ell(\xi_1)\theta^0_\ell) \tag{17}$$

$$f^0_2 = x_2 = \phi_\ell(\xi_1)X_{\ell 2} + \frac{h_0}{2}\xi_2\sin(\phi_\ell(\xi_1)\theta^0_\ell) \tag{18}$$

$$f^1_1 = y_1 = \phi_\ell(\xi_1)Y_{\ell 1} + \frac{h_0}{2}\xi_2\cos(\phi_\ell(\xi_1)\theta^1_\ell) \tag{19}$$

$$f^1_2 = y_2 = \phi_\ell(\xi_1)Y_{\ell 2} + \frac{h_0}{2}\xi_2\sin(\phi_\ell(\xi_1)\theta^1_\ell) \tag{20}$$

The unknown parameters per each node $\ell$ are three, i.e., two current positions $Y_{\ell i}$ and one rotation $\theta^1_\ell$. Function $f^0_i$ is used to find $A^0$ while function $f^1_i$ is used to find $A^1$ (trial). The composition of these two values for each integration station (Gauss for instance) gives the numerical value of the deformation gradient for any initial geometry (curved) with any order of approximation. Forces are the energy conjugates of positions, so the natural conjugate of rotation is the momentum.

It is worth to show the derivatives of $f^1_i$ regarding the non-dimensional variables, constituting the gradient $A^1_{ij}$ as follows:

$$A^1_{11} = \phi_{\ell,1}(\xi_1)Y_{1\ell} - \frac{h_0}{2}\xi_2\sin(\phi_\ell(\xi_1)\theta^1_\ell)\phi_{\ell,1}(\xi_1)\theta^1_\ell \tag{21}$$

$$A^1_{21} = \phi_{\ell,1}(\xi_1)Y_{2\ell} + \frac{h_0}{2}\xi_2\cos(\phi_\ell(\xi_1)\theta^1_\ell)\phi_{\ell,1}(\xi_1)\theta^1_\ell \tag{22}$$

$$A^1_{12} = \frac{h_0}{2}\cos(\phi_\ell(\xi_1)\theta^1_\ell) \tag{23}$$

$$A^1_{22} = \frac{h_0}{2}\sin(\phi_\ell(\xi_1)\theta^1_\ell) \tag{24}$$

The derivatives of $A^1$ regarding nodal parameters are used in the next section, so the non-zero values of the first and second derivatives are given as follows:

$$\frac{\partial A^1_{11}}{\partial Y_{1k}} = \phi_{(k),1}(\xi_1) \tag{25}$$

$$\frac{\partial A^1_{11}}{\partial \theta^1_k} = -\frac{h_0}{2}\xi_2 \cos(\phi_\ell(\xi_1)\theta^1_\ell)\phi_k(\xi_1)\phi_{\ell,1}(\xi_1)\theta^1_\ell - \frac{h_0}{2}\xi_2 \sin(\phi_\ell(\xi_1)\theta^1_\ell)\phi_{k,1}(\xi_1) \tag{26}$$

$$\frac{\partial A^1_{21}}{\partial Y_{2k}} = \phi_{(k),1}(\xi_1) \tag{27}$$

$$\frac{\partial A^1_{21}}{\partial \theta^1_k} = -\frac{h_0}{2}\xi_2 \sin(\phi_\ell(\xi_1)\theta^1_\ell)\phi_k(\xi_1)\phi_{\ell,1}(\xi_1)\theta^1_\ell + \frac{h_0}{2}\xi_2 \cos(\phi_\ell(\xi_1)\theta^1_\ell)\phi_{k,1}(\xi_1) \tag{28}$$

$$\frac{\partial A^1_{12}}{\partial \theta^1_k} = -\frac{h_0}{2} \sin(\phi_\ell(\xi_1)\theta^1_\ell)\phi_k(\xi_1) \tag{29}$$

$$\frac{\partial A^1_{22}}{\partial \theta^1_k} = \frac{h_0}{2} \cos(\phi_\ell(\xi_1)\theta^1_\ell)\phi_k(\xi_1) \tag{30}$$

The non-zero second derivatives are:

$$\begin{aligned}\frac{\partial^2 A^1_{11}}{\partial \theta^1_k \partial \theta^1_m} &= \frac{h_0}{2}\xi_2 \sin(\phi_\ell(\xi_1)\theta^1_\ell)\phi_m(\xi_1)\phi_k(\xi_1)\phi_{\ell,1}(\xi_1)\theta^1_\ell - \frac{h_0}{2}\xi_2 \cos(\phi_\ell(\xi_1)\theta^1_\ell)\phi_m(\xi_1)\phi_{k,1}(\xi_1) \\ &- \frac{h_0}{2}\xi_2 \cos(\phi_\ell(\xi_1)\theta^1_\ell)\phi_k(\xi_1)\phi_{m,1}(\xi_1)\end{aligned} \tag{31}$$

$$\begin{aligned}\frac{\partial^2 A^1_{21}}{\partial \theta^1_k \partial \theta^1_m} &= \frac{h_0}{2}\xi_2 \cos(\phi_\ell(\xi_1)\theta^1_\ell)\phi_m(\xi_1)\phi_k(\xi_1)\phi_{\ell,1}(\xi_1)\theta^1_\ell - \frac{h_0}{2}\xi_2 \sin(\phi_\ell(\xi_1)\theta^1_\ell)\phi_{k,1}(\xi_1)\phi_m(\xi_1) \\ &- \frac{h_0}{2}\xi_2 \sin(\phi_\ell(\xi_1)\theta^1_\ell)\phi_k(\xi_1)\phi_{m,1}(\xi_1)\end{aligned} \tag{32}$$

$$\frac{\partial^2 A^1_{12}}{\partial \theta^1_k \partial \theta^1_m} = -\frac{h_0}{2} \cos(\phi_\ell(\xi_1)\theta^1_\ell)\phi_k(\xi_1)\phi_m(\xi_1) \tag{33}$$

$$\frac{\partial^2 A^1_{22}}{\partial \theta^1_k \partial \theta^1_m} = -\frac{h_0}{2} \sin(\phi_\ell(\xi_1)\theta^1_\ell)\phi_k(\xi_1)\phi_m(\xi_1) \tag{34}$$

In the next section, all degrees of freedom are called simply $Y_{\ell i}$, with $i$ varying from 1 to 3. Translations are related to $i = 1, 2$ and rotations to $i = 3$. When $\ell$ is not present in an equation it means that the element number is omitted.

## 4 DYNAMIC NONLINEAR FORMULATION WITH DUMPING AND NON-CONSERVATIVE FORCES

The conservation of energy in a mechanical system is guaranteed if the input and output of energy are at balance. If there is some kind of dissipation the total energy of the system changes along time. It can be understood writing the total potential energy of a system as follows:

$$\Pi = \Pi_0 - Q(t,x) \tag{35}$$

where $Q(t,x)$ can be stated as the quantity of energy withdrawn from the simple conservative idealized energy $\Pi_0$ [16]. In this work the non-conservative forces will be considered as part of this dissipative potential. As a consequence, $\Pi$ is the remaining (current) mechanical energy of the system. Equation (35) can be rewritten as:

$$\Pi_0 = \Pi + Q(t,x) \tag{36}$$

This equation can be understood as recovering the possibility of using stationary properties for the mechanical system analysis, i.e., one can use the minimum potential energy theorem on the energy function $\Pi_0$ for equilibrium analysis.

For a structural problem associated with a fixed reference system, figure 4, the ideal potential energy function can be written as the composition of the strain energy ($U_e$), the potential energy of applied conservative forces (P), the kinetic energy ($K$) and dissipation ($Q$), as follows.

$$\Pi_0 = U_e - \mathrm{P} + K + Q \tag{37}$$

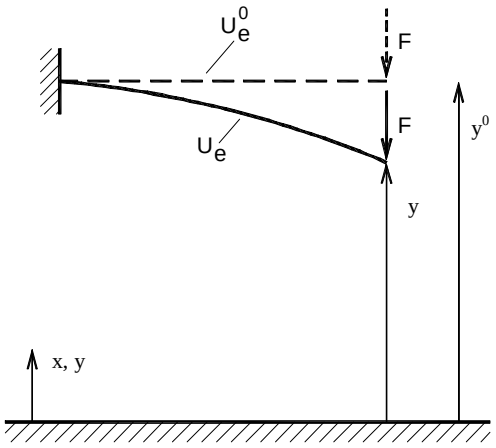


Figure 4 Total Potential Energy written for a body in two different positions.

The strain energy function of the body, frame for instance, is considered stored in the initial volume of the body ($V0$) and is written as an integral of the specific strain energy value ($u_e$), equation (3), as

$$U_e = \int_{V_0} u_e dV_0 \tag{38}$$

The strain energy is assumed to be zero in the initial position, called non-deformed. The potential energy of the applied conservative forces is written as:

$$P = F_i Y_i + \int_{s_0} t_i y_i ds^0 \tag{39}$$

where $F_i$ represents forces (or moments) applied in "i" direction and $Y_i$ is the ith current position of the point where the load is applied, $t_i$ is the distributed force applied in "i" direction and $y_i$ is the current position of mid line points ($i = 3$ is avoided for distributed forces). The symbol $ds_0$ represents the initial differential length of elements. The kinetic energy is written as

$$K = \frac{1}{2} \int_{V_0} \rho_0 \dot{y}_i \dot{y}_i dv_0 \tag{40}$$

where $\dot{y}_i$ are velocities and $\rho_0$ is the mass density, relative to the initial volume $V_0$. The dissipative term, including non conservative distributed forces, is written in its differential form as

$$\frac{\partial}{\partial y_i} Q(t, y) = \int_{v_0} \frac{\partial}{\partial y_i} \bar{q}(y, t) dv_0 = \int_{v_0} \lambda_m \rho_0 \dot{y}_i dv_0 - \int_{s_0} q_i ds_0 \tag{41}$$

where $\bar{q}$ is the specific dissipative functional, $\lambda_m$ is a proportionality constant, $\dot{y}_i$ are velocities of any point and $q_i$ are non conservative distributed forces given by:

$$q_1 = \mathrm{q_t} \sin(\phi_\ell(\xi_i) Y_{\ell 3}) + \mathrm{q_n} \cos(\phi_\ell(\xi_i) Y_{\ell 3}) \tag{42}$$

$$q_2 = \mathrm{q_n} \sin(\phi_\ell(\xi_i) Y_{\ell 3}) - \mathrm{q_t} \cos(\phi_\ell(\xi_i) Y_{\ell 3}) \tag{43}$$

Where $q_n$ and $q_t$ are respectively the normal and tangential distributed forces over the element and $Y_{\ell 3}$ is the rotation of nodes. For balloons analysis $q_n$ is the internal pressure, usually called $p$. The integral of dissipative forces respects the direction of the current position but its integral is performed over the initial length as the load magnitudes ($q_n$ and $q_t$) are written regarding initial position. The current load is easily known by multiplying these magnitudes by $\det(A)$, for usual applications of thin unstable structures the value of $\det(A) \cong 1$.

Substituting equations (38), (39) and (40) in equation (37) results in

$$\Pi_0 = \int_{V_0} u_e dV_0 - F_i Y_i - \int_{s_0} t_i y_i ds_0 + \frac{1}{2} \int_{V_0} \rho_0 \dot{y}_i \dot{y}_i dV_0 + Q \tag{44}$$

This energy function can be evaluated substituting the exact position field by its approximation described in section 3, i.e.:

$$\Pi_0 = \int_{V_0} u_e(\xi_1, Y_i) dV_0 - F_i Y_i - \int_{s_0} t_i y_i(\xi_1, Y_i) ds_0 + \frac{1}{2} \int_{V_0} \rho_0 \dot{y}_i \dot{y}_i(\xi_1, Y_i) dV_0 + Q(\xi, Y_i) \tag{45}$$

The minimum potential energy theorem is used in $\Pi_0$ by differentiating equation (45) regarding a generic nodal position $Y_{\ell j}$, which results in

$$\frac{\partial \Pi_0}{\partial Y_{\ell j}} = \int_{V_0} \frac{\partial u_e(\xi_1, Y_i)}{\partial Y_{\ell j}} dV_0 + \int_{V_0} \rho_0 \phi_{\ell j}(\xi_1)\phi_{ki}(\xi_1) dV_0 \ddot{Y}_{ki} + \int_{V_0} \lambda_m \rho_0 \phi_{\ell j}(\xi_1)\phi_{ki}(\xi_1) dV_0 \dot{Y}_{ki} - F_{\ell j} - \\ - \int_{s_0} \phi_{\ell j}(\xi_1)\phi_{ki}(\xi_1) ds_0 t_{ki} - \int_{s_0} q_j \phi_{\ell j}(\xi_1) ds_0 = 0 \tag{46}$$

It is worth noting that this time the dissipative potential is differentiated regarding nodal positions, differently of the described in equation (41). Equations (42) and (43) should be introduced in the last integral of equation (46) to perform the numerical integration.

One can rewrite equation (46) in a simple vector form as

$$g_{\ell j} = \frac{\partial U_e}{\partial Y_{\ell j}} + F_{\ell j}^{inert.} + F_{\ell j}^{damp.} - F_{\ell j}^{c} - F_{\ell j}^{nc} = 0 \tag{47}$$

or

$$g_{\ell j} = \frac{\partial U_e}{\partial Y_{\ell j}} + M\ddot{Y}_{\ell j} + C\dot{Y}_{\ell j} - F_{\ell j}^{c} - F_{\ell j}^{nc} = 0 \tag{48}$$

The involved forces are, inertial force $F_{\ell j}^{inert.}$or $M\ddot{Y}_{\ell j}$, dumping $F_{\ell j}^{damp.}$or $C\dot{Y}_{\ell j}$ and the external force, divided into conservative $F_{\ell j}^{c}$ and non-conservarive $F_{\ell j}^{nc}$. Splitting the derivative of the specific strain energy, one writes:

$$\frac{1}{2}\frac{\partial}{\partial Y_{\ell j}}\left(E_{kl} C_{k\,\mathrm{lim}} E_{im}\right) = \frac{1}{2}\frac{\partial}{\partial E_{\alpha\beta}}\left(E_{kl} C_{k\,\mathrm{lim}} E_{im}\right)\frac{\partial E_{\alpha\beta}}{\partial Y_{\ell j}} = C_{\alpha\beta im} E_{im}\frac{\partial E_{\alpha\beta}}{\partial Y_{\ell j}} = S_{\alpha\beta}\frac{\partial E_{\alpha\beta}}{\partial Y_{\ell j}} \tag{49}$$

Consequently:

$$F_{\ell j}^{int.} = \int_{V_0} C_{\alpha\beta im} E_{im}\frac{\partial E_{\alpha\beta}}{\partial Y_{\ell j}} dV_0 \tag{50}$$

where $F_{\ell j}^{int}$ is the first gradient vector of the strain energy potential, understood as internal force. Equation (47) means that if the internal force vector is equal to the applied one the solid is at equilibrium. If not, vector $g_{\ell j}$ can be understood as the unbalanced force of the mechanical system.

The current position is the unknown of the problem, so it is necessary to solve the non-linear equation (47) regarding $Y_{\ell j}$ and time. The first step is to integrate it along time using the Newmark $\beta$ method and then apply the Newton Rapson procedure, as described in the next section.

## 5 TIME MARCHING PROCESS AND PLACECITYNEWTON RAPSON PROCEDURE

From the previous developments equation (47) can be written in a simpler vector form as

$$g = \frac{\partial U_e}{\partial Y} - F^c - F^{nc} + M\ddot{Y} + C\dot{Y} = 0 \tag{51}$$

Expression (51) represents the dynamic equilibrium equation at any time and has to be solved. In order to do so the first step is to write the equilibrium for a specific instant $(S+1)$, as follows:

$$\left.\frac{\partial \Pi}{\partial Y}\right|_{S+1} = \left.\frac{\partial U_e}{\partial Y}\right|_{S+1} - F_{S+1} + M\ddot{Y}_{S+1} + C\dot{Y}_{S+1} = 0 \tag{52}$$

Applying the Newmark $\beta$ approximations [1] for position description one has:

$$Y_{S+1} = Y_S + \Delta t\dot{Y}_S + \Delta t^2\left[\left(\frac{1}{2} - \beta\right)\ddot{Y}_S + \beta\ddot{Y}_{S+1}\right] \tag{53}$$

$$\dot{Y}_{S+1} = \dot{Y}_S + \Delta t\left(1-\gamma\right)\ddot{Y}_S + \gamma\Delta t\ddot{Y}_{S+1} \tag{54}$$

Substituting approximations (53) and (54) into equation (52) results in

$$g\left(Y_{S+1}\right) = \left.\frac{\partial \Pi}{\partial Y}\right|_{S+1} = \left.\frac{\partial U_e}{\partial Y}\right|_{S+1} - F_{S+1} + \frac{M}{\beta\Delta t^2}Y_{S+1} - MQ_S + CR_S + \frac{\gamma C}{\beta\Delta t}Y_{S+1} - \gamma\Delta tCQ_S = 0 \tag{55}$$

where vectors $Q_s$ and $R_s$ represent the dynamic contribution of the past, and are given by

$$Q_S = \frac{Y_S}{\beta\Delta t^2} + \frac{\dot{Y}_S}{\beta\Delta t} + \left(\frac{1}{2\beta} - 1\right)\ddot{Y}_S \tag{56}$$

$$R_S = \dot{Y}_S + \Delta t\left(1-\gamma\right)\ddot{Y}_S \tag{57}$$

Equation (55) can be understood simply by $g\left(Y_{S+1}\right) = 0$ and is clearly non-linear in $\left(Y_{S+1}\right)$. A Taylor expansion to solve this non-linear equation regarding positions is necessary. It is important to mention that the non-conservative force vector is also dependent of current positions, however at this step it will be considered constant in order to achieve a symmetric matrix. The rate of convergence of the resulting iterative process may suffer some prejudice; however the overall processing time is reduced due to symmetry and less computational effort to build matrices.

The second derivative of the total energy potential is then given by:

$$\left.\frac{\partial^2 \Pi}{\partial Y^2}\right|_{S+1} = \nabla g\left(Y_{s+1}\right) = \left.\frac{\partial^2 U_e}{\partial Y^2}\right|_{S+1} + \frac{M}{\beta\Delta t^2} + \frac{\gamma C}{\beta\Delta t} \tag{58}$$

And one builds the placeCityTaylor series of first order as:

$$0 = g(Y) \cong g\left(Y^0\right) + \nabla g\left(Y^0\right)\Delta Y \tag{59}$$

and derives the Newton-Raphson procedure to solve the non-linear equation (55), i.e.,

$$\nabla g\left(Y^0\right)\Delta Y = -g\left(Y^0\right) \tag{60}$$

where $Y^0$ is a trial position (usually $Y_s$) for $Y_{s+1}$ used in equation (55) to calculate $g\left(Y^0\right)$. Solving $\Delta Y$ one calculates a new trial for $Y_{s+1}$ as

$$Y_{S+1} = Y^0 + \Delta Y \tag{61}$$

The acceleration must be corrected by an expression obtained from equation (53), i.e.,

$$\ddot{Y}_{S+1} = \frac{Y_{S+1}}{\beta\Delta t^2} - Q_S \tag{62}$$

This equation is used in equation (54) to correct velocity. The stop criterion is given in equation (63), when a chosen tolerance ($TOL$) is satisfied.

$$\left\|g(Y^0)\right\| \leq TOL \tag{63}$$

It must be noted that, before the first time step, the initial acceleration must be calculated as follows

$$\ddot{Y}_0 = M^{-1}\left[F_0 - \left.\frac{\partial U_e}{\partial Y}\right|_0 - C\dot{Y}_0\right] \tag{64}$$

The Newmark parameters ($\gamma$ and $\beta$) can be chosen in order to achieve a stable algorithm. For instance, using constant acceleration for a time step ($\gamma$=*0.50* and $\beta$=*0.25*) the unconditional stability is obtained [9, 17].

## 6 THE DERIVATIVES OF THE SPECIFIC STRAIN ENERGY

In order to conclude the formulation the second derivatives of the strain energy regarding nodal positions should be explicitly shown as it has been done for the first derivative in equation (50). From equations (49) and (50) one writes, using index notation:

$$\frac{\partial^2 U_e}{\partial Y_k \partial Y_j} = \int_{V_0} \frac{\partial}{\partial Y_k}\left(C_{\alpha\beta im}E_{im}\frac{\partial E_{\alpha\beta}}{\partial Y_j}\right)dV_0 = \int_{V_0}\left(\frac{\partial E_{im}}{\partial Y_k}C_{\alpha\beta im}\frac{\partial E_{\alpha\beta}}{\partial Y_j} + E_{im}C_{\alpha\beta im}\frac{\partial^2 E_{\alpha\beta}}{\partial Y_j \partial Y_k}\right)dV_0 \tag{65}$$

Finally, the first and second derivatives of the Green strain regarding current nodal positions should be done. Firstly the necessary derivatives of the Cauchy-Green stretch tensor are presented. Next the derivatives of strains are straightforward achieved. Recalling that the Cauchy-Green stretch tensor is given by:

$$C = A^t A \tag{66}$$

and omitting, for simplicity, extra indices, one applies the positional FEM mapping and writes:

$$C = [(A^0)^t]^{-1}(A^1)^t(Y_i)A^1(Y_i)(A^0)^{-1} \tag{67}$$

Remembering that $A_0$ is constant regarding the current position, the first derivative is performed as:

$$\frac{\partial C}{\partial Y_j} = [(A^0)^t]^{-1}\frac{\partial (A^1)^t(Y_i)}{\partial Y_j}A^1(Y_i)(A_0)^{-1} + [(A^0)^t]^{-1}(A^1)^t(Y_i)\frac{\partial A^1(Y_i)}{\partial Y_j}(A^0)^{-1} \tag{68}$$

For which the values of $\frac{\partial A^1(Y_i)}{\partial Y_j}$ are given at the end of section 3. In this section $Y_j$ is not represented in bold case because it follows index notation for which $j$ represents a global degree of freedom.

The second derivative of the Cauchy-Green stretch is given by,

$$\begin{aligned}\frac{\partial^2 C}{\partial Y_j \partial Y_k} &= [(A^0)^t]^{-1}\frac{\partial (A^1)^t(Y_i)}{\partial Y_j}\frac{\partial A^1(Y_i)}{\partial Y_k}(A_0)^{-1} + [(A^0)^t]^{-1}\frac{\partial (A^1)^t(Y_i)}{\partial Y_k}\frac{\partial A^1(Y_i)}{\partial Y_j}(A^0)^{-1} + \\ &+[(A^0)^t]^{-1}\frac{\partial^2 (A^1)^t(Y_i)}{\partial Y_j \partial Y_k}A^1(Y_i)(A_0)^{-1} + [(A^0)^t]^{-1}(A^1)^t(Y_i)\frac{\partial^2 A^1(Y_i)}{\partial Y_j \partial Y_k}(A^0)^{-1}\end{aligned} \tag{69}$$

Where $\partial^2 A^1/\partial Y_j \partial Y_k$ is given at the end of section 3. Recalling equation (2), one achieves the first and second derivatives of the Green strain directly as

$$\frac{\partial E}{\partial Y_j} = \frac{1}{2}\frac{\partial C}{\partial Y_j}; \frac{\partial^2 E}{\partial Y_j \partial Y_k} = \frac{1}{2}\frac{\partial^2 C}{\partial Y_j \partial Y_k} \tag{70}$$

It is important to mention that the present technique can be applied to any strain measure based on the Cauchy-Green stretch. Equations (55), (58) and (60) indicate that the proposed procedure can be operated by means of creating a Hessian matrix and global internal forces for finite elements and composing the global matrix and internal force vector by summation of coincident degrees of freedom, as it is done for usual FEM procedures. One should remember that all nodal parameters follow the global system of reference, avoiding the use of rotation schemes.

## 7 NUMERICAL EXAMPLES

This section provides some selected examples in order to verify the good behavior of the proposed formulation when dealing with general problems, mainly very thin inflatable structures. It is important to note that the first example is a benchmark of literature used to prove the capability o the proposed formulation to model all the necessary inertial characteristics of large rotation situations, proving the positional formulation able to be applied to high speed problems. The other examples are dedicated to very thin and inflatable structures, in order to test the formulation for further three dimensional analyses of balloons.

## 7.1 Spin-up maneuver

The first numerical example is a simple fixed flexible beam, a benchmark of non-linear dynamic formulations. It has been presented in several references, see for instance [12, 13, 20]. The spin-up-maneuver is subject to a turn function ($\psi(t)$), applied on the restricted node, see figure 5.

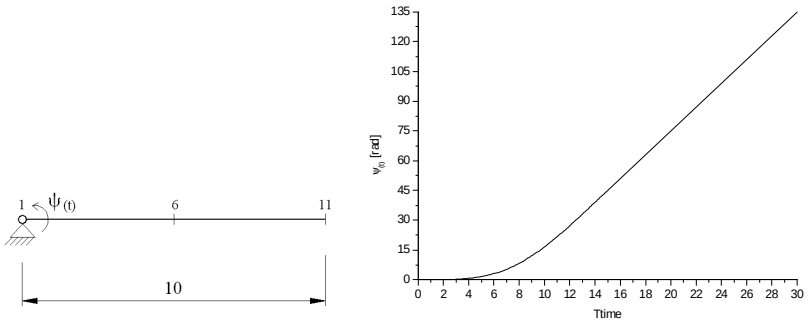


Figure 5 Flexible spin-up maneuver input data.

The adopted non-dimensional parameters for the beam are, EI=1.4 $10^4$, EA=2.8 $10^7$, $\rho$I=6.0 $10^{-4}$, $\rho$A=1.2. This type of turn function represents a typical helicopter blade rotation. The structure is approximated by a mesh of 5 finite elements with quadractic approximation. The final result is compared to an analytical value demonstrating that all effects, for this kind of analysis, have been captured.

The expressions of the turn function are presented in equations (71) and (72).

$$\psi(t) = \frac{2}{5}\left[\frac{t^2}{2} + \left(\frac{15}{2\pi}\right)^2\left(\cos\frac{2\pi t}{15} - 1\right)\right] rad \qquad 0 \le t \le 15 \tag{71}$$

$$\psi(t) = (6t - 45)\, rad \qquad t > 15 \tag{72}$$

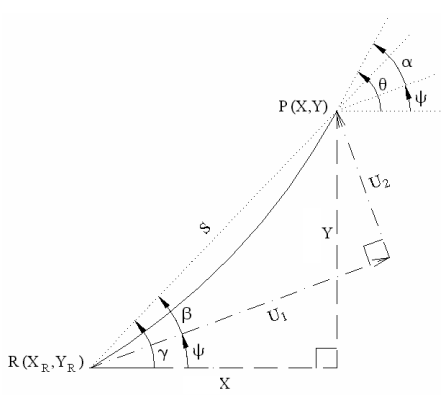


Figure 6 Shape configurations and local system of coordinates.

In figure 6 the rigid body motion deformed configurations are presented. A local system of co-ordinates is created to compare results, where the displacements $U_1$ and $U_2$ are measured.

From positions $X$ and $Y$, and the rotation ($\theta$) of the extreme node it is possible to calculate the displacements $U_1$ and $U_2$, and the relative rotation ($\alpha$) between the deformed configuration and the rigid body motion, as follows.

$$S = \sqrt{X^2 + Y^2} \tag{73}$$

$$\beta = \gamma - \psi \tag{74}$$

$$U_1 = S\cos\beta - 10 \tag{75}$$

$$U_2 = Ssen\beta \tag{76}$$

$$\alpha = \theta - \psi \tag{77}$$

Figures 7, 8 and 9 present displacements $U_1$ and $U_2$, and the relative rotation $\alpha$, respectively, compared to analytical final values. The analytical value for $U_1$ is given by $U_1 = \rho(d\psi/dt) * R^3/(6E)$, the others are trivial.

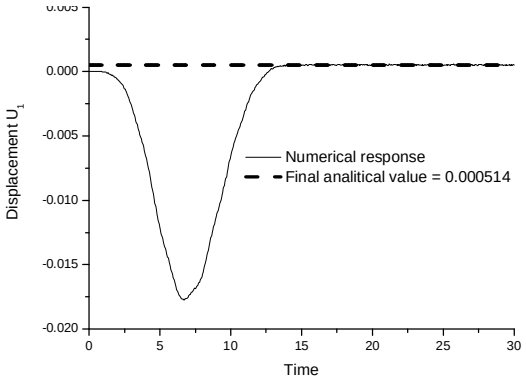


Figure 7 Displacement $U_1$.

Figure 10 present the deformed shapes and the rigid body motions of the structure for some instants during the first cycle. The achieved results are in total agreement with references [12, 13, 20].

## 7.2 Column buckling

This example is introduced here just to show that the present non-linear formulation is very accurate to capture the critical load of slender structures subjected to compressive loads. The

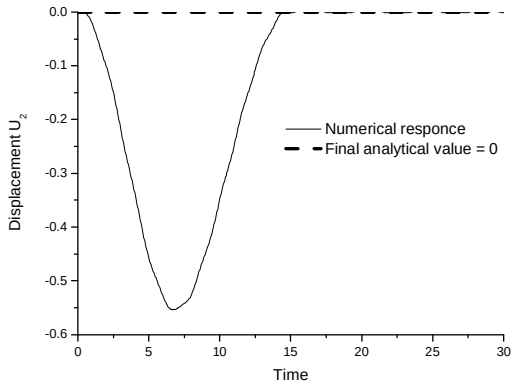


Figure 8 Displacement $U_2$.

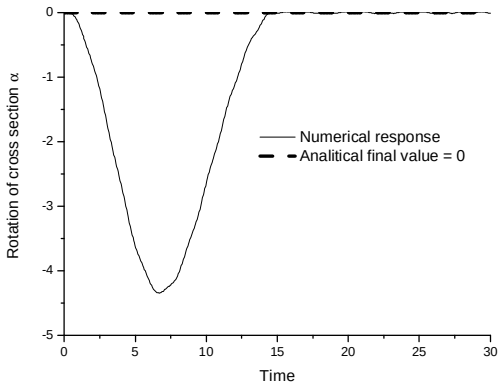


Figure 9 Relative rotation angle $\alpha$.

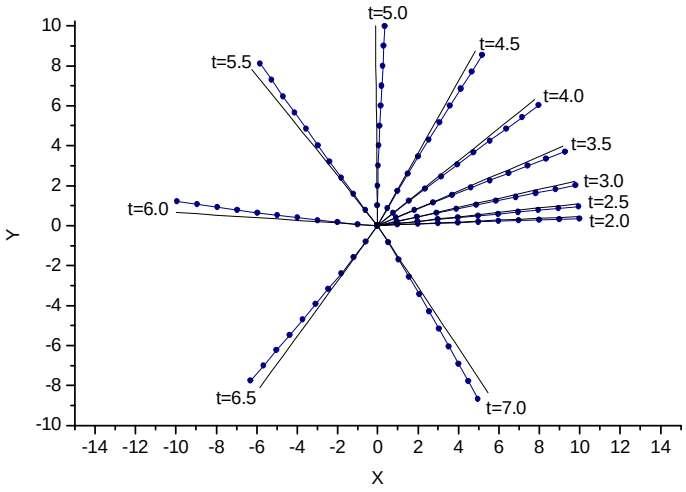


Figure 10 Flexible beam, deformed shapes (–■–) and rigid body motions (—-).

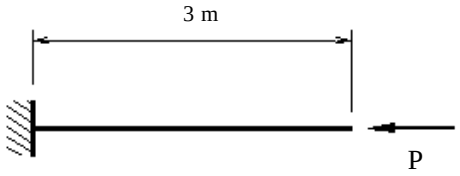


Figure 11 Dimensions and loading for the column.

analyzed column has the following properties: $l = 3m$, $E = 3.5x10^6 kg/(s^2\, mm)$, $h = 2.5mm$ and $b = 1.0\, mm$, see figure 11.

The applied load $P = 9.9946\, kg\, mm/s^2$ is divided into 200 load steps and two discretizations are used, one with 5 elements of 3 nodes (quadratic) and other with 2 elements of 6 nodes (fifth order). The same results are achieved for both formulations. Figure 12 shows the lateral displacement of the loaded point of the column versus the applied load and the theoretical value of the critical load ($P_{cr} = 4.9973\, kg\, mm/s^2$). As one can see these values coincide perfectly at the load step 100.

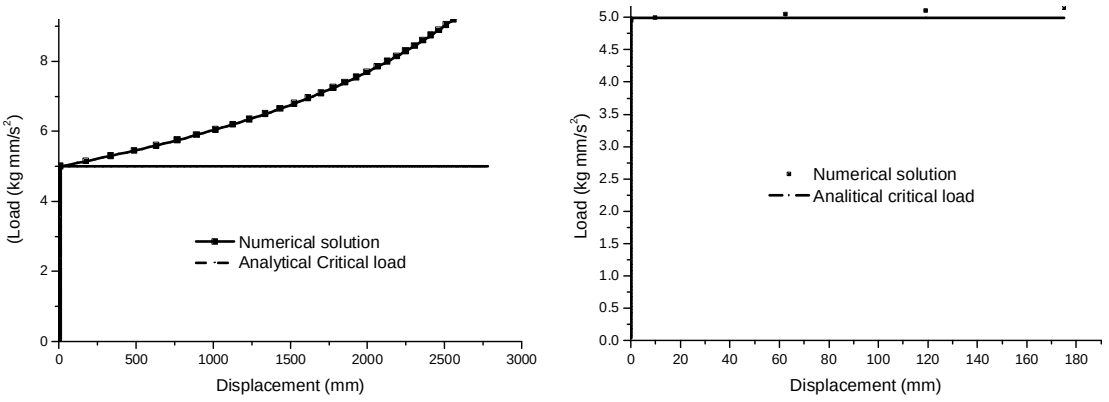


(a) General view (b) Closer view

Figure 12 Critical value definition.

## 7.3 Negative pressure applied in a cylindrical balloon

The folding (post-buckling behavior) of an infinitely long cylindrical balloon is analyzed assuming a 2D formulation, see figure 13. Both static and dynamic formulations are used to develop the analysis. The properties of the balloon are: $R = 3m$, $E = 3.5x10^6 kg/(s^2\, mm)$, $h = 0.04mm$, $\rho = 4.7x10^{-7} kg/mm^3$ and $b = 100mm$. The material (unless the Poisson ratio) corresponds to a polymeric material, Kampton® [24, 25], that has great importance in aerospace engineering. Using the static formulation the first critical load is achieved and compared to a simplified analytical solution (sinusoidal mode). For the static analysis, double symmetry is employed together with 61 nodes. Two different element degrees were adopted, 20 elements of third order (4 nodes each) and 10 elements of sixth order (7 nodes each).

The total negative pressure, see figure 13, is applied in 300 load steps and the buckling occurs at step 250 for both discretizations, corresponding to a critical load of $p_{cr} = 2.50x10^{-9}kg/(s^2\,mm)$, see figure 14. The sinusoidal analytical value is $p_{\sin} = 2.765x10^{-9}kg/(s^2\,mm)$. In figure 14 one can see the influence of a sinusoidal defect imposed into de radius of the initial configuration, the defect is applied correcting the initial configuration by the formulae$R = R+D\,\cos(2\theta)$ in which $D$ is the maximum defect value. One can see that the balloon behaviour is very sensitive to the initial configuration (following the value of variable $D$).

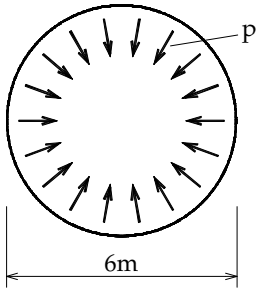


Figure 13 Initial geometry and loading.

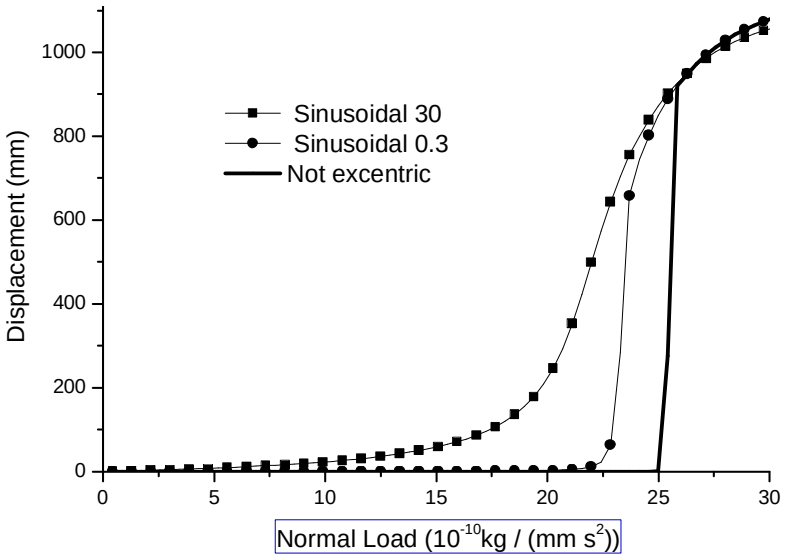


Figure 14 Maximum lateral displacement versus applied force, defect influence.

For the sake of completeness, figure 15 shows the sinusoidal buckling mode and the achieved numerical mode and reveals that a maximum difference of only 1.1% in the buckling shape can generate almost 15% of difference in the critical load determination.

The dynamic analysis is used to determine the influence of the load rate regarding time in the path chosen by the balloon to de-inflate. This influence is a physical characteristic of dynamic systems, i.e., to change the trajectory of a body developing a straight path with a

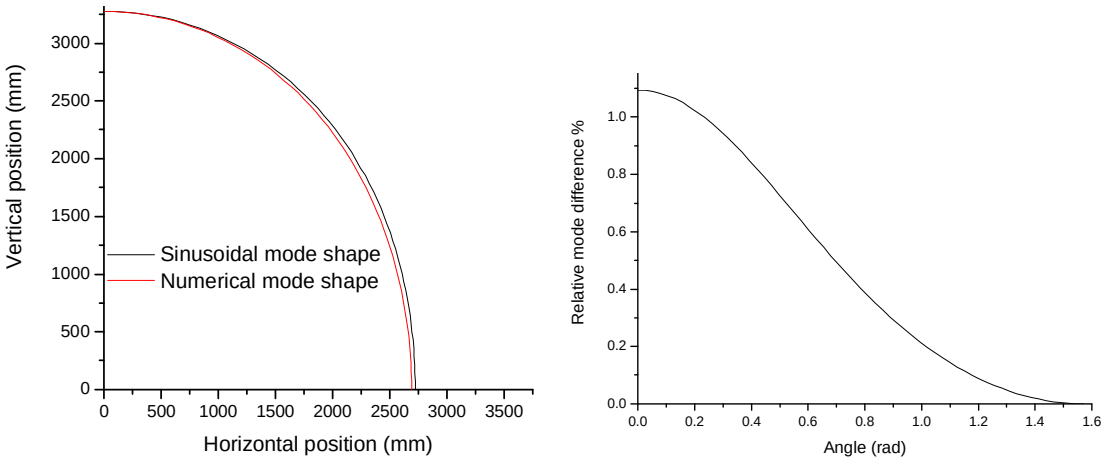


(a) Buckling modes (b) Relative mode difference

Figure 15 Buckling modes and relative difference.

determined velocity it is necessary to apply a force component orthogonal to the pre-defined path. In the case of the studied balloon, there is no tangential unbalanced force unless the ones generated by the numerical error. This error is responsible for the static buckling depicted in figure 14. In the dynamic case, it is expected that, if the de-inflation velocity is large enough when the body is passing through the first buckling mode, the balloon will not wrinkle and will pass trough to the next buckling mode and so on.

To test this property the rate of the applied load is varied. In figures 16 to 20 the paths for some load rates are depicted. Symmetry is not used, as the plane of symmetry of general modes are not the same. The adopted time step is $\Delta t = 0.5s$, large enough to filtrate undesired small membrane vibrations. The applied load is proportional to time, i.e., $p(t) = a\,t$, where $a$ is the load rate. No dumping is considered.

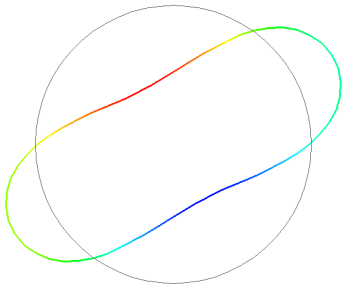

Figure 16 Applied load rate $a = 0.27x10^{-12}(Kg/(mm\,s^2))/s$, load level at the deformed configuration $p = 3.25x10^{-9}Kg/(mm\,s^2)$.

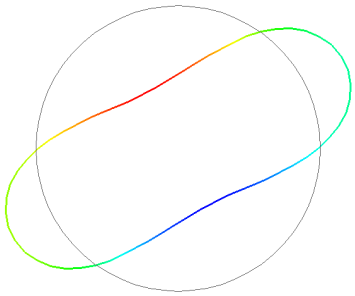

Figure 17 Applied load rate $a$ = $0.27x10^{-11}(Kg/(mm\,s^2))/s$, load level at the deformed configuration $p$ = $8.64x10^{-9}Kg/(mm\,s^2)$.

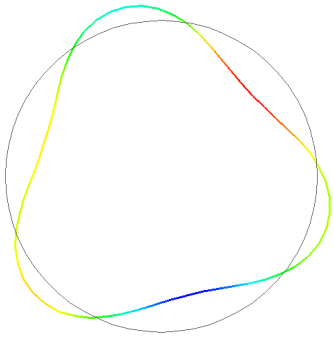

Figure 18 Applied load rate $a$ = $1.35x10^{-11}(Kg/(mm\,s^2))/s$, load level at the deformed configuration $p$ = $1.89x10^{-8}Kg/(mm\,s^2)$.

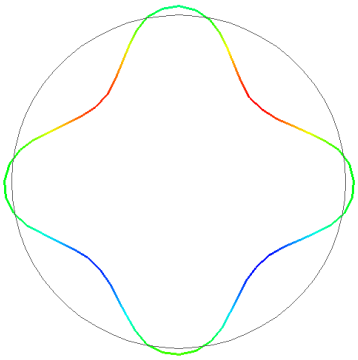

Figure 19 Applied load rate $a$ = $0.27x10^{-10}(Kg/(mm\,s^2))/s$, load level at the deformed configuration $p$ = $2.592x10^{-8}Kg/(mm\,s^2)$. For rate $a$ = $0.27x10^{-9}(Kg/(mm\,s^2))/s$ the path is the same.

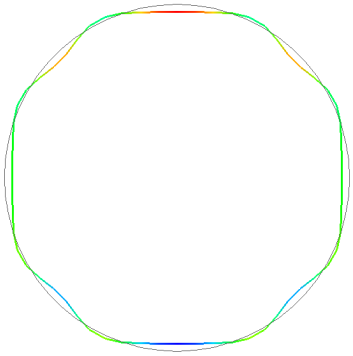

Figure 20 Applied load rate $a$ = $0.27x10^{-8}(Kg/(mm\,s^2))/s$, load level at the deformed configuration $p$ = $2.43x10^{-7}Kg/(mm\,s^2)$.

One can see from figures 16 to 20 that as the load rate grows the activated mode is higher. Sometimes it is possible to find mixed modes. In figure 20, modes three and four are mixed. From this analysis one can observe that the simulation of balloons or any other unstable structure is a difficult task and depends on the quality of the known information. Moreover the proposed formulation is able to capture the expected behavior of this kind of structure for negative pressure.

### 7.4 De-inflating of a cylindrical balloon

The same balloon of example 6.3 is slowly de-inflated over a frictionless half-space. At the beginning of analysis the balloon is at an initial position without self weight and internal pressure. Constant and equal internal pressure (to inflate) and self weight values are applied, following a linear growth regarding time. The load time rate is $2x10^{-9}kg/(mm\,s^2)/s$ from time 0 to time $40s$. After that, from time $40s$ to time $48s$ the self weight is maintained constant and the internal pressure falls to 0. From time $48s$ to time $68s$ only the self weight acts and is considered constant. The adopted time step is $\Delta t$ = $0.001s$ and the advantage of simple symmetry is taken. Fifty curved elements with 4 nodes each are used to model the structure, resulting in 151 nodes. The following figures depict some positions for selected instants. No dumping is considered.

As one can see the presence of the self weight and the horizontal surface leads the structure to a slow de-inflation without the occurrence of natural buckling modes.

### 7.5 Fast inflation and taking off of a balloon

The same balloon of the previous example is subjected to an internal pressure and self weight allowing its' taking off. At the beginning of analysis the balloon is at an initial position without self weight and internal pressure. This time the self weight and the internal pressure varies regarding time following the same rate $2x10^{-9}kg/(mm\,s^2)/s$ until 40s, however the spatial pattern of internal pressure is not constant, but follows a proportion of 1 at the bottom and 2 at the top of the balloon regarding the self weight. After 40s the self weight is maintained

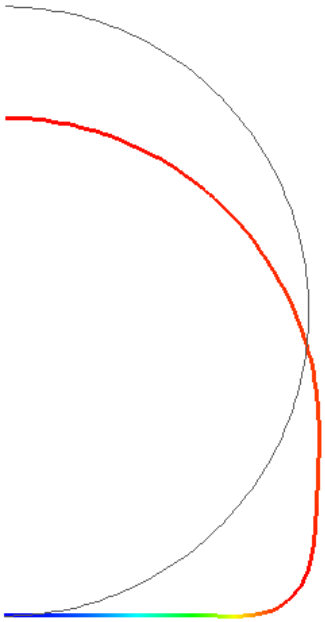

Figure 21 Position for time $40s$.

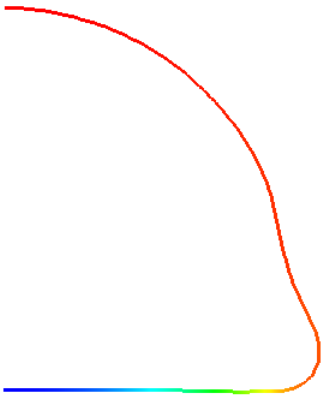

Figure 22 Position for time $48s$.

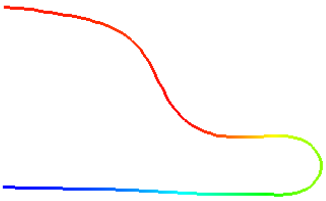

Figure 23 Position for time $58s$.

Figure 24 Position for time $68s$.

constant and the internal pressure starts to grow in a rate ten times the initial rate until time 112s. A proportional dumping constant of $\lambda_m = 0.01s^{-1}$ is adopted. Some stages of the balloon taking off are shown in figure 25.

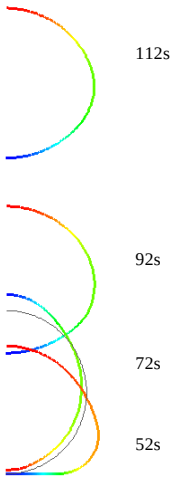


Figure 25 ???????

As one can see, during the first 52s of the analysis the balloon is de-inflating, after this it inflates quickly and takes off. This kind of balloon, without openings and heavy weights on its bottom tends to stabilize as a pumpkin balloon.

### 7.6 Natural shape balloon

This time the same material and initial position of the previous balloons is considered, but it has been adopted different varying pressure patterns regarding vertical position. The vertical variations are: square root, linear, quadratic and cubic from zero at the bottom to one at the top. The self weight is neglected and no horizontal surface is considered. The Bottom of the balloon is considered fixed and free to rotate, simulating a balloon with heavy weight and a small opening at the bottom. The internal pressure rate is $2x10^{-6}kg/(mm\,s^2)/s$ inflating. The adopted time step is $\Delta t = 0.015s$ with dumping $1.0s^{-1}$. Figures 26 to 29 present the initial and final (stable) configurations of the balloon for different pressure patterns. The coarse quality (in pixels) of the adopted in house post processing shows trembling lines, however they are quite smooth.

This example shows that the balloon shape changes as the pattern of internal pressure changes. Therefore it is important to know the behavior of internal pressure at different altitudes the balloon assumes in atmosphere. Moreover, for a initially spherical balloon the stable position should be like the ones presented above, however the balloon will reduce its hemisphere at its bottom (zero pressure region), indicating the importance of example 6.3, where compressive stress develops. The 3D formulation to be implemented should be capable of capturing all these effects.

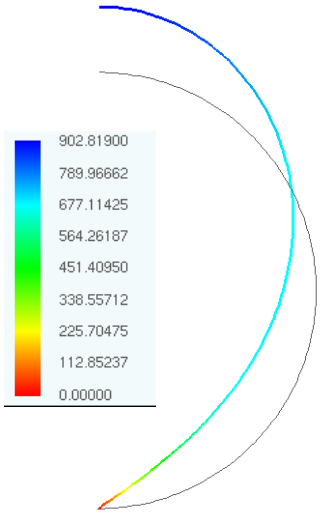


Figure 26 Shape and vertical displacement for square root pressure pattern.

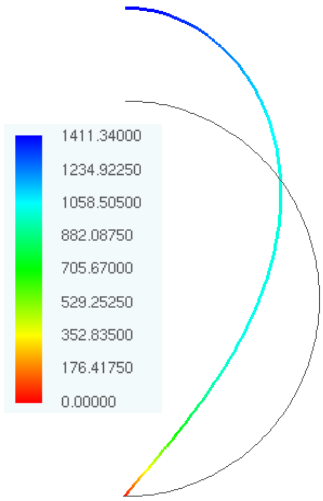


Figure 27 Shape and vertical displacement for linear pressure pattern.

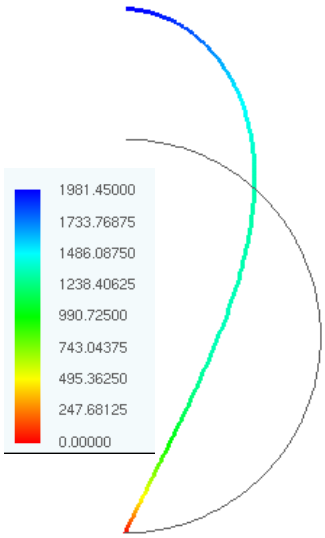


Figure 28 Shape and vertical displacement for quadratic pressure pattern.

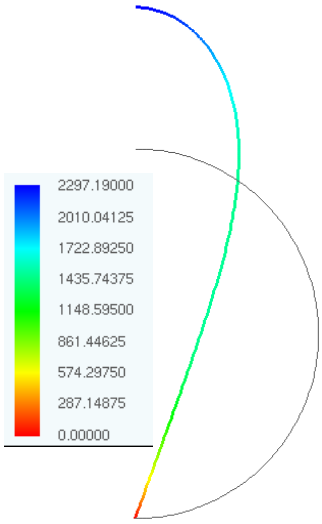


Figure 29 Shape and vertical displacement for cubic pressure pattern.

## 8 CONCLUSIONS

A new, simple and robust formulation to solve dynamic geometrical non-linear problems with large deflections applied to very thin and inflatable 2D structures has been proposed. The formulation is based on position description, simplifying the understanding and the implementation of large deflection analysis when compared to typical FEM formulations. The Newmark time integration scheme has been successfully applied to integrate positions along time. The results for benchmark structures are in good agreement with literature. The presented results show that the proposed formulation is suitable to solve dynamic geometrical nonlinear problems with large deflection and rotations, including contact and very thin inflate structures (balloons). The formulation is promising and should be extended to three dimensions and further applications.

**Acknowledgements** The author would like to acknowledge CNPq (National Counsel of Technological and Scientific Development) for the financial support given to this research.

## References

[1] J. Argyris and H. P. Mlejnek. *Dynamics of structures, Texts on computational mechanics*, volume 5. North-Holland, Amsterdam, 1991.

[2] F. Baginski and W. Schur. Structural analysis of pneumatic envelopes: A variational formulation and optimization-based solution process. *AIAA Journal*, 41(2):304–311, 2003.

[3] F. Baginski, K. Brakke, and W. W. Schur. Cleft formation in pumpkin balloons. *Adv. Space Res.*, 37:2070–2081, 2006.

[4] F. E. Baginski. On the design and analysis of inflated membranes: natural shape and pumpkin shaped balloons. *SIAM J. Appl. Math.*, 65(3):838–857, 2005.

[5] M. Bischoff and E. Ramm. On the physical significance of higher order kinematic and static variables in a three-dimensional shell formulation. *International Journal of Solids and Structures*, 37(46-47):6933–6960, Nov 2000.

[6] P. G. Ciarlet. *Mathematical Elasticity*. North Holland, 1993.

[7] H. B. Coda and R. R. Paccola. An alternative positional FEM formulation for geometrically non-linear analysis of shells – curved triangular isoparametric elements. *Computational Mechanics*, 40(1):185–200, 2007.

[8] H. B. Coda and R. R. Paccola. A positional FEM formulation for geometrical non-linear analysis of shells. *Latin American Journal of Solids and structures*, 5(3):205–223, 2008.

[9] H. B. Coda and R. R. Paccola. Unconstrained finite element for geometrical non-linear dynamics of shells. *Mathematical Modelling in Engineering*, 2009.

[10] M. A. Crisfield. A consistent corotational formulation for nonlinear, 3-dimensional, beam-elements. *Computer methods in applied mechanics and engineering*, 81:131–150, 1990.

[11] M. A Crisfield. *Non-Linear finite element analysis of solids and structures*, volume 1. John Wiley & Sons, England, 1991.

[12] H. A. Elkaranshawy and M. A. Dokainish. Corotational finite element analysis of planar flexible multibody systems. *Computer & structures*, 54:881–890, 1995.

[13] M. Greco and H. B. Coda. Positional FEM formulation for flexible multi body dynamic analysis. *Journal of Sound and Vibration*, 2006.

[14] M. Greco, F. A. R. Gesualdo, H. B. Coda, and W. S. Venturin. Nonlinear positional formulation for space truss analysis. *Finite Element analysis and design*, 2006.

[15] T. R. Kane, R. R. Ryan, and A. K. Banerjee. Dynamic of a beam attached to a moving base. *Astrodynamic Specialist Conference*, AAS:85–390, 1986.

[16] C. Lanczos. *The variacional principles of mechanics*. Dover, New York, 4 edition, 1970.

[17] R. W. Ogden. *Non-linear Elastic deformation*. Ellis Horwood, England, 1984.

[18] A. C. Pipkin. Relaxed energy densities for large deformations of membranes. *IMA Journal of Applied Mathematics*, 52:297–308, 1994.

[19] J. C. Simo and L. Vu-Quoc. On the dynamics of flexible beams under large overall motions – the plane case: part 1. *Journal of applied mechanics, ASME*, 53:849–854, 1986.

[20] J. C. Simo and L. Vu-Quoc. On the dynamics of flexible beams under large overall motions – the plane case: part 2. *Journal of applied mechanics, ASME*, 53:855–863, 1986.

[21] J. C. Simo and L. Vu-Quoc. The role of non-linear theories in transient dnamic analysis of flexible structures. *Journal of Sound and Vibration*, 119:487–508, 1987.

[22] D. J. Steigman and A. C. Pipkin. Axisymmetric tension fields. *ZAMP*, 40:526–542, 1989.

[23] M. Stein and J. M. Hedgepath. Analysis of partially wrinkled membranes. *NASA TN D-813*, 1961.

[24] Y. W. Wong and S. Pellegrino. Wrinkled membranes part I: Experiments. *Journal of Mechanics of Materials and Structures*, 1:1–23, 2006.

[25] Y. W. Wong and S. Pellegrino. Wrinkled membranes part III: Numerical simulation. *Journal of Mechanics of Materials and Structures*, 1:61–93, 2006.

[26] P. Wriggers and J. C. Simo. A general procedure for the direct computation of turning and bifurcation points. *International journal for numerical methods in engineering*, 30:155–176, 1990.